Chapter 2
Radiology and Diagnostic Approaches to Sinonasal Malignancies and Skull Base Tumors

Michael Marino, Joseph M. Hoxworth, Devyani Lal, and Valerie J. Lund

Introduction

Diagnosis of sinonasal malignancies and skull base tumors involves evaluation of the patient's symptoms, nasal endoscopy findings, and radiographic imaging. Diagnostic algorithms, in combination with clinical judgment, allow for a systematic approach and are tailored for malignant (Fig. 2.1) and benign sinonasal tumors (Fig. 2.2). In most instances, biopsy is necessary for definitive diagnosis, and a systematic diagnostic approach can guide how and where to obtain tissue.

Radiologic imaging is an essential component for evaluation of patients with suspected or known sinonasal malignancies and skull base tumors. Imaging can aid in differentiating neoplasm from inflammatory disease, as well as benign and malignant tumors. To this extent radiology complements history, physical exam, and nasal endoscopy findings as part of a complete diagnostic algorithm. Sinonasal malignancies represent less than 5% of all head and neck cancers, but these are comprised of over 20 histopathologies [1, 2]. The simultaneous rarity and pathologic diversity can present a diagnostic challenge, which can be partially resolved by interpretation of different imaging modalities. Furthermore, a multidisciplinary team provides the necessary radiological expertise for the diagnosis and management of sinonasal and skull base tumors [3, 4].

Imaging is central to disease staging. Tumor-node-metastasis (TNM) staging is the most broadly applicable system, although alternate classifications are relevant

M. Marino (✉) · D. Lal
Otolaryngology – Head & Neck Surgery, Mayo Clinic, Phoenix, AZ, USA
e-mail: marino.michael@mayo.edu

J. M. Hoxworth
Radiology, Mayo Clinic, Phoenix, AZ, USA

V. J. Lund
Professorial Unit, Royal National Throat, Nose and Ear Hospital, London, UK

N. F. Saba, D. T. Lin (eds.), *Sinonasal and Skull Base Malignancies*,
https://doi.org/10.1007/978-3-030-97618-7_2

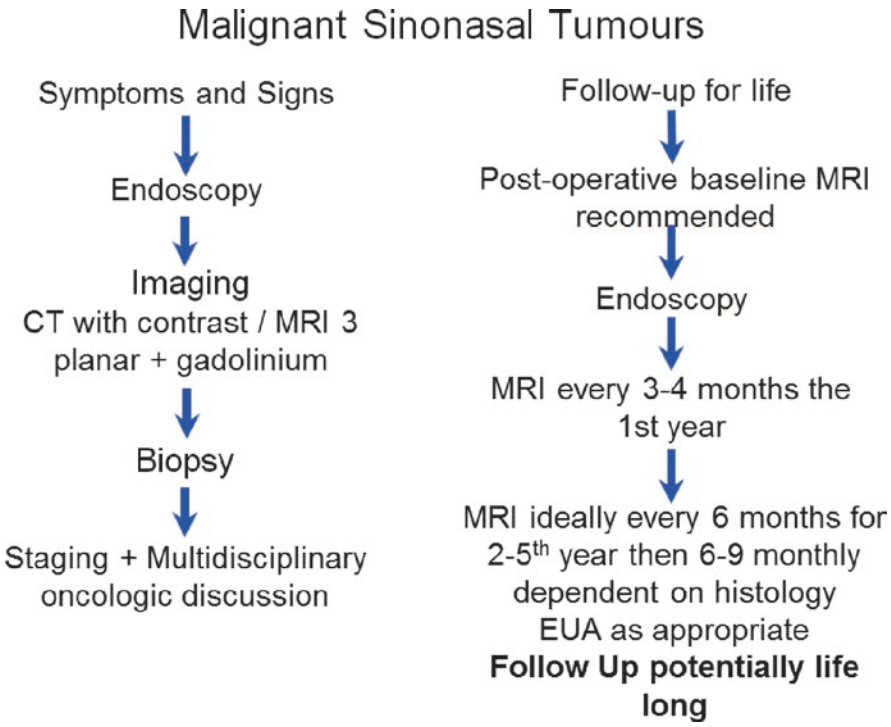

Fig. 2.1 Diagnostic and follow-up algorithm for sinonasal malignancy. (Adapted from European Position Paper on Endoscopic Management of Tumors of Nose, Sinuses, and Skull Base [3])

for specific histopathologies. Beyond disease stage, imaging defines anatomical involvement for detailed surgical and radiation field planning. High resolution and multiplanar reconstructions available in modern imaging modalities allow for assessment of tumor involvement of critical structures, including orbital and intracranial extension, internal carotid artery encasement, dural venous sinus invasion, and perineural spread. The combined use of relevant imaging modalities is critical for complete assessment of local anatomical involvement and disease stage, and for planning therapeutic interventions.

Nasal Endoscopy and Biopsy

Following history and physical exam, nasal endoscopy is the initial diagnostic intervention for identification of a sinonasal mass. Comprehensive endoscopy includes visualization of the nasal cavity, middle meatus, superior meatus, sphenoethmoid recess, and nasopharynx. Anterior rhinoscopy is a useful part of the physical exam, although nasal endoscopy substantially improves the diagnostic accuracy [5].

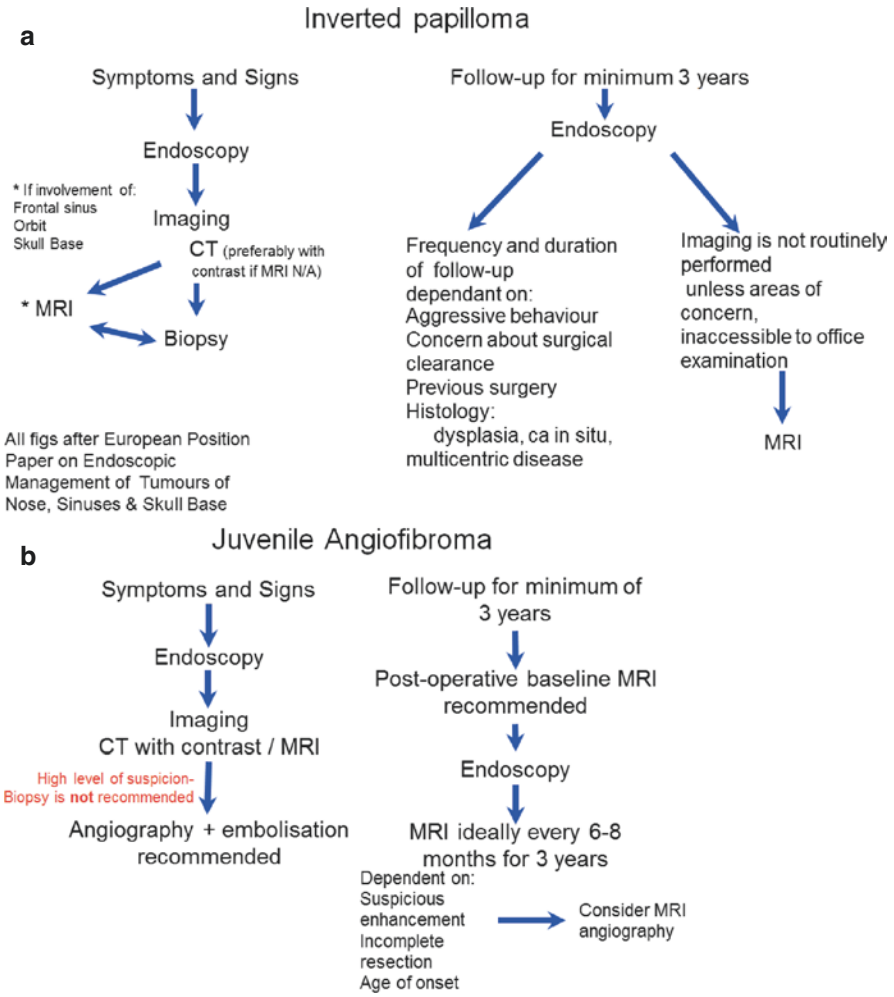

Fig. 2.2 Diagnostic and follow-up algorithm for (**a**) inverted papilloma and (**b**) juvenile angiofibroma. (Adapted from European Position Paper on Endoscopic Management of Tumors of Nose, Sinuses, and Skull Base [3])

Visualization of an abnormal appearing mass or lesion in the sinonasal cavities can also guide obtaining additional imaging, though associated inflammation and edema may obscure the view. Nasal endoscopy can be helpful for mapping the extent of the visualized portions of the tumor, while radiographic imaging defines the deep extent [6].

Biopsy is required in most cases in order to definitively establish the histopathologic diagnosis. Evaluation of a suspected mass with additional imaging is recommended prior to performing biopsy, as certain imaging characteristics may identify lesions where biopsy is challenging or contraindicated. For instance, if juvenile

angiofibroma is suspected by history, endoscopy, and imaging features, biopsy would be contraindicated in favor of angiography and embolization. Similarly, imaging characteristics consistent with encephalocele would be a contraindication for biopsy. Challenging situations such as highly vascular lesions or high risk for cerebrospinal fluid (CSF) leak may require formal exam under anesthesia, rather than tissue biopsy in the office setting.

Tissue obtained during biopsy prior to treatment can also be used for genomic and immunohistochemical analyses that may have prognostic value and identify therapeutic targets. Genome-wide DNA methylation profiling, copy number analysis, and immunohistochemistry have been described for the classification of sinonasal malignancies, including intestinal-type adenocarcinoma, olfactory neuroblastoma, and sinonasal undifferentiated carcinoma (SNUC) [7–9]. Using these techniques to subgroup tumors according to genomic or proteomic profile may be beneficial in predicting tumor behavior. Furthermore, personalized therapies can be based on these profiles with directed monoclonal antibodies or small molecule inhibitors.

Computed Tomography

Computed tomography (CT) is frequently the first line imaging modality in the evaluation of sinonasal symptoms, and interpretation of suggestive findings is an initial step for the diagnosis of sinonasal malignancies and skull base tumors. CT findings may also guide obtaining additional imaging and magnetic resonance imaging (MRI) in particular, in order to improve soft tissue characterization and to define tumor site of origin and extent. Features on CT that generally prompt suspicion for a neoplastic process include unilateral sinus opacification, bony remodeling/erosion (Fig. 2.3a), sclerosis or aggressive periostitis (Fig. 2.3b), and frankly invasive behavior (Fig. 2.3c) [6, 10]. Unilateral sinus opacification has been associated with benign and malignant neoplasms with an odds ratio of 7.8 and 8, respectively [11]. Similar associations were reported when a single sinus was affected [11]. Enlargement of skull base foramina may be associated with perineural spread (Fig. 2.3d). Furthermore, when imaging of the neck is included, lymphadenopathy can be suggestive of malignant disease (Fig. 2.3e), which is associated with certain histopathologies such as malignant melanoma, squamous cell carcinoma, and esthesioneuroblastoma [6]. Triplanar and contrast-enhanced images are preferable in the setting of a known sinonasal mass or unilateral nasal endoscopy findings, although interpretation of noncontrast images may be necessary when scans were obtained for general evaluation of sinonasal symptoms. Additional CT features can be useful for evaluating specific pathologies and tumor extent for staging purposes.

There are characteristic CT findings for several benign sinonasal lesions. Hyperostosis apparent on imaging has been described as the site of origin for

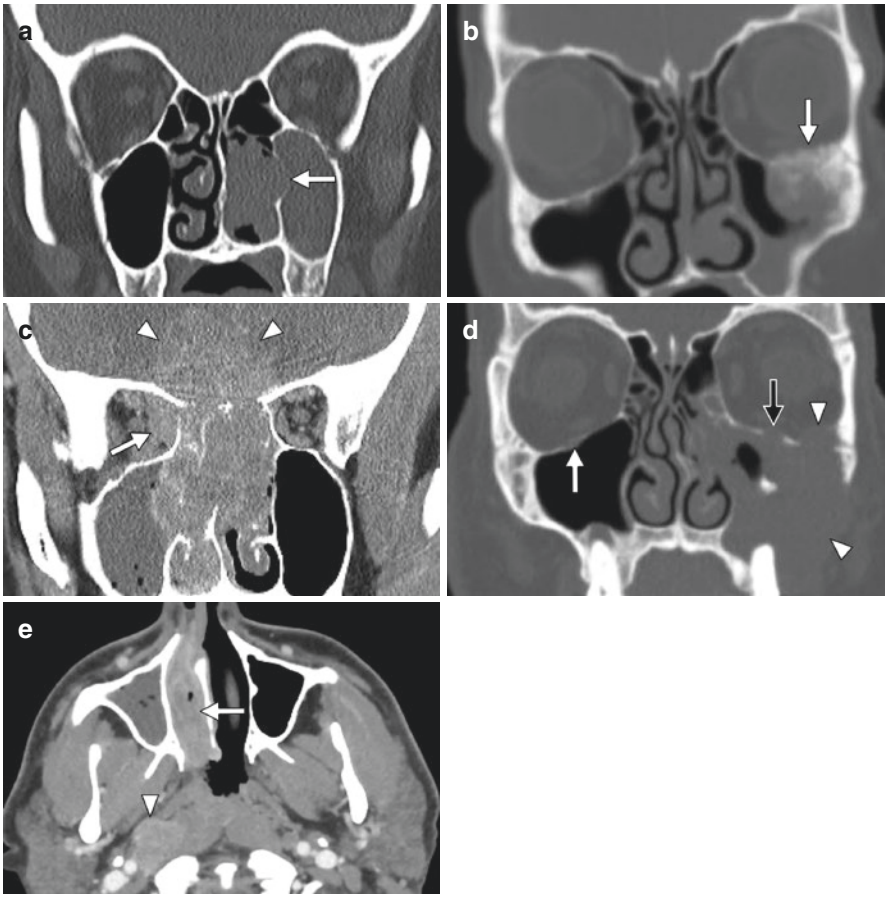

Fig. 2.3 CT features that raise suspicion for malignancy within an opacified sinus. (**a**) A 79-year-old woman with sinonasal melanoma. Left-sided nasal mass causes smooth bone remodeling and erosion (arrow) in the medial wall of the left maxillary sinus. Although mucocele and benign neoplasms can cause a similar pattern of osseous change, a nonaggressive and indolent appearance does not exclude malignancy. (**b**) A 63-year-old man with squamous cell carcinoma. The pattern of opacification in the left maxillary sinus is nonspecific, but the aggressive pattern of periosteal new bone formation along the left orbital floor (arrow) is highly concerning for an underlying malignancy. (**c**) A 29-year-old man with esthesioneuroblastoma. Although MRI offers superior soft tissue contrast, CT in this case clearly illustrates that a large sinonasal mass is invading the right orbit (arrow) and the anterior cranial fossa (arrowheads). (**d**) A 46-year-old man with squamous cell carcinoma. In addition to bone destruction involving the left maxillary sinus and orbital floor (arrowheads) suggesting malignancy, the left infraorbital canal is abnormally expanded by perineural spread of carcinoma (black arrow), as compared with the normal right infraorbital canal (white arrow). (**e**) A 42-year-old woman with esthesioneuroblastoma. An abnormally enlarged and heterogeneously enhancing right retropharyngeal lymph node (arrowhead) is concerning for metastatic disease and therefore significantly increases the likelihood that the mass opacifying the right nasal cavity (arrow) is malignant

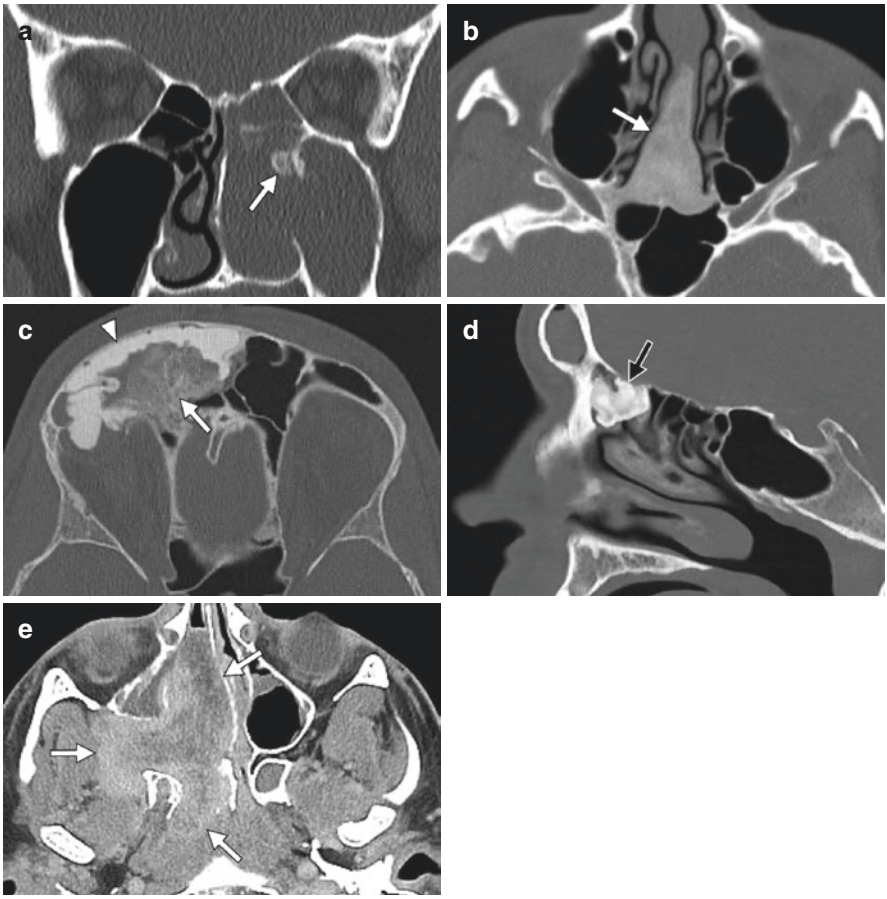

Fig. 2.4 CT findings associated with benign sinonasal masses/expansile lesions. (**a**) A 48-year-old man with inverted papilloma. Although not entirely specific, focal hyperostosis (arrow) at the point of attachment is a recognized feature of inverted papilloma. (**b**) A 21-year-old woman with fibrous dysplasia. Expansile lesion along the nasal septum and basisphenoid (arrow) has a homogeneous "ground-glass" density that is very characteristic of fibrous dysplasia. (**c**) A 22-year-old man with ossifying fibroma. Expansile ossific mass remodeling the right frontal sinus is densely sclerotic anterolaterally (arrowhead) and more intermediate in density posteriorly (arrow). From an imaging standpoint, a "mixed" osteoma could have a similar appearance when containing both cortical and cancellous bones. (**d**) A 35-year-old man with osteoma. Densely calcified frontoethmoidal mass (arrow) is compatible with an "ivory" osteoma. (**e**) A 16-year-old man with juvenile angiofibroma. A large avidly enhancing nasal and nasopharyngeal mass (arrows) has widened and remodeled the region of the right sphenopalatine foramen and pterygopalatine fossa, ultimately reaching the infratemporal fossa

inverted papillomas (Fig. 2.4a) [12, 13]. Calcifications within the tumor may be seen, although findings of necrosis are suggestive of malignant transformation [10]. Fibro-osseous lesions include osteoma, fibrous dysplasia, and ossifying fibroma, and the nature and extent of these lesions can be determined using CT. Fibrous

dysplasia often appears as a "ground-glass" expansile more diffuse lesion (Fig. 2.4b), while ossifying fibroma appears as a well-circumscribed lesion with sclerotic margins (Fig. 2.4c) [14]. An osteoma is again a circumscribed lesion that typically has a homogeneous, dense osseous appearance (Fig. 2.4d) though the degree of calcification can vary [14]. Juvenile angiofibroma has pathognomonic radiological appearances that obviate the need for biopsy (Fig. 2.4e) [15]. There is consistently erosion of the bone of the posterior margin of the sphenopalatine foramen extending to the base of the medial pterygoid plate reflecting the site of origin of the lesion. Ninety-six percent have enlargement or erosion of the vidian canal [16], 83% extension into the sphenoid sinus, and 64% enlargement of the pterygomaxillary fissure and extension to the infratemporal fossa. Anterior bowing of the posterior wall of the maxillary sinus is seen in ~80% of cases on axial CT though this must be distinguished from any slow-growing lesion in the infratemporal fossa such as a schwannoma, hemangiopericytoma, or rhabdomyosarcoma. These features together with non-opacification of the maxillary sinus differentiate angiofibromas from antrochoanal polyps. Pleomorphic adenoma most commonly arise from the nasal septum and are associated with bony remodeling [6], while schwannomas present as hypodense soft tissue masses within the ethmoid or maxillary sinuses, or nasal cavity [10].

Squamous cell carcinoma is the most common malignant histology, and is one of the most common sinonasal malignancies [6, 10, 17, 18]. CT findings of squamous cell carcinoma are nonspecific, although bone erosion is a general sign of malignancy (Fig. 2.3b). When compared with sinonasal lymphoma, squamous cell carcinoma was more likely to have findings of bony destruction [18]. Cervical nodal or distant metastases are uncommon and seen in less than 20% of cases at presentation but should be considered [6, 10]. Adenocarcinoma is difficult to distinguish from squamous cell carcinoma on the basis of CT features alone, although adenocarcinomas more frequently arise in the ethmoid sinuses and superior nasal cavity while squamous cell carcinoma is more commonly located in the maxillary sinus or nasal cavity [19]. Salivary gland tumors including adenoid cystic carcinomas are also without CT-specific findings.

Olfactory neuroblastoma or esthesioneuroblastoma is a malignancy of neural crest origin, arising from the olfactory mucosa. Low-grade tumors are expansile with remodeling of adjacent bone, although high-grade variants result in bony destruction (Fig. 2.3c) [6, 10]. Calcifications may also be seen within the tumor on CT [10]. On imaging olfactory neuroblastoma is typically seen within or arising from the olfactory cleft, although ectopic lesions have been reported [20]. Imaging of the neck is recommended as cervical lymphadenopathy is found in ~23% during the course of the disease (Fig. 2.3e) [21]. Sinonasal endocrine carcinoma (SNEC), sinonasal undifferentiated carcinoma (SNUC), and NUT carcinoma are also sinonasal malignancies with neuroendocrine features. These tumors are more aggressive with invasive features on CT, as well as more frequent distant or nodal metastases. Sinonasal melanoma is also a tumor of neural crest origin, and imaging often does not correlate with the aggressive behavior and high recurrence rate. Homogeneous

contrast enhancement is seen on CT, and bony remodeling is typically seen (Fig. 2.3a) rather than aggressive bone destruction [6, 10].

Non-Hodgkin lymphoma comprises the vast majority of sinonasal lymphoma, and is classified into B-cell and T-/NK-cell subtypes. B-cell lymphomas are more common in Western populations, while T-/NK-cell lymphomas are more frequently seen in Asian populations [10, 19]. In B-cell lymphomas, bulky masses with homogeneous contrast enhancement are common CT findings (Fig. 2.5a) [19]. Sinonasal lymphomas have also been shown to have increased tumor volume compared to squamous cell carcinoma [17]. T-/NK-cell lymphomas, however, are often associated with extensive bony and soft tissue destruction, potentially leading to diagnostic confusion with other destructive conditions such as granulomatosis with polyangiitis and invasive fungal disease [6].

Sarcomas are an additional group of malignancies that may be encountered in the sinonasal region. Osteosarcoma and chondrosarcoma have been removed from the most recent World Health Organization (WHO) classification of sinonasal tumors, as these histopathologies were felt to be adequately described elsewhere [1]. Nevertheless, osteosarcoma and chondrosarcoma can present in the sinonasal cavity or skull base, in addition to other sarcomatous tumors such as rhabdomyosarcoma and biphenotypic sinonasal sarcoma.

Osteosarcomas are associated with osteoid matrix and characteristic "sunburst" periosteal reaction (Fig. 2.5b), although this is not present in all cases [6]. Chondrosarcoma is most commonly found to arise from the nasal septum for nasal cavity lesions, extending superiorly into the anterior and midskull base or inferiorly into the hard palate, while the petroclival synchondrosis is the most common site for skull base lesions [22]. Skull base chondrosarcoma can be differentiated from chordoma, as chondrosarcoma is more likely to have eccentric position in the clivus due to origin from the petroclival synchondrosis. When present within a chondrosarcoma, chondroid matrix often has a curvilinear appearance on CT that has been likened to "rings and arcs" (Fig. 2.5c). Rhabdomyosarcoma demonstrates simultaneous bony remodeling and erosion on CT. These tumors are typically homogeneous with moderate enhancement. Biphenotypic sinonasal carcinoma has been recently described, and demonstrates both myogenic and neural features. CT findings include mixed lytic and sclerotic patterns with internal calcification (Fig. 2.5d) [10, 23]. Biphenotypic sinonasal carcinoma is found to most frequently involve the nasal and ethmoid cavities [23].

Metastatic lesions to the sinonasal cavity from distant sites are uncommon, but known to occur. Renal cell carcinoma is the most frequent primary tumor of sinonasal metastasis but they may also arise from breast, lung, prostate, testis, and thyroid. Spread of cutaneous malignancy, including squamous cell carcinoma, basal cell carcinoma, and melanoma, to the sinonasal cavity is also recognized. Metastases from primaries elsewhere are typically centered on bony structures of the sinonasal tract with erosive changes. These areas should be considered during systemic imaging for staging.

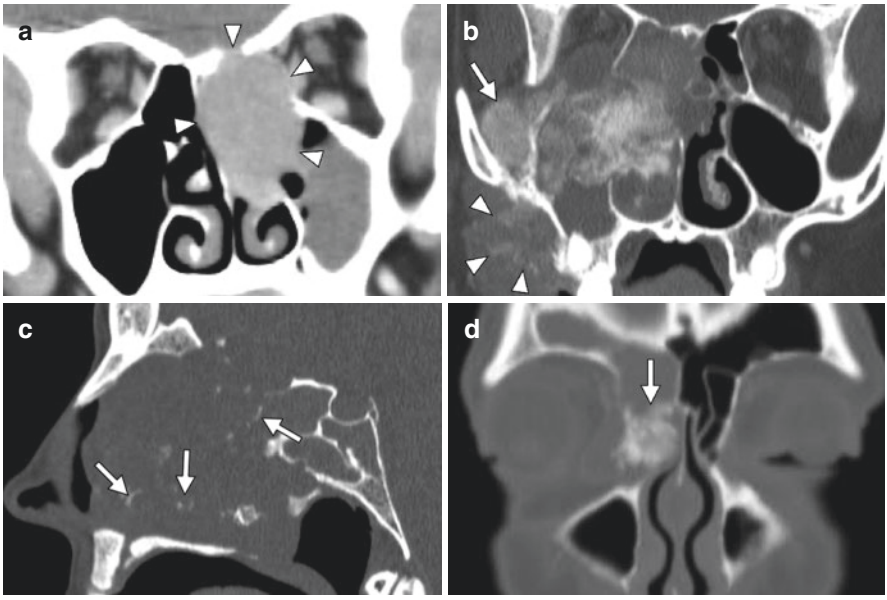

Fig. 2.5 CT characteristics of non-carcinomatous malignancies. (**a**) A 28-year-old woman with primary sinonasal diffuse large B-cell lymphoma. A large diffusely enhancing sinonasal mass erodes the lamina papyracea, medial maxillary sinus wall, nasal septum, and ethmoid roof (arrowheads). A carcinoma of similar size would tend to enhance less homogeneously due to focal areas of necrosis. (**b**) A 25-year-old woman with maxillary osteosarcoma. In association with this large destructive sinonasal mass, note the presence of relatively homogeneous osteoid matrix (arrow) as well as an aggressive pattern of periosteal new bone formation (arrowheads), which has been radiographically described as a "sunburst" pattern. (**c**) A 62-year-old woman with low-grade chondrosarcoma. As seen in the sagittal plane, the large sinonasal mass contains multiple calcifications, some of which are curvilinear in appearance (arrows). The latter have been described as "rings and arcs" when associated with chondroid matrix. (**d**) A 58-year-old woman with biphenotypic sinonasal sarcoma. Focal intratumoral calcification (arrow) seen in this right anterior nasoethmoidal mass is a frequently reported feature of this rare tumor type

Computed Tomography Angiography

Computed tomography angiography (CTA) can be a useful adjunct in the evaluation of sinonasal and skull base tumors, particularly when surgical resection is being considered [24]. CTA allows for assessment of the tumor extent in relation to important bony and vascular structures, most notably the internal carotid artery (Fig. 2.6a, b). Visualization of draining venous sinuses (such as the cavernous sinus) is also possible. Vascular encasement or loss of bony covering due to tumor invasion can be determined in order to plan surgery and the feasibility of resection. Furthermore, noninvasively defining the vascular anatomy with CTA will determine whether endovascular interventions are indicated prior to surgery. High-resolution (≤1 mm axial slice thickness) CTA images with triplanar reconstructions can also be used

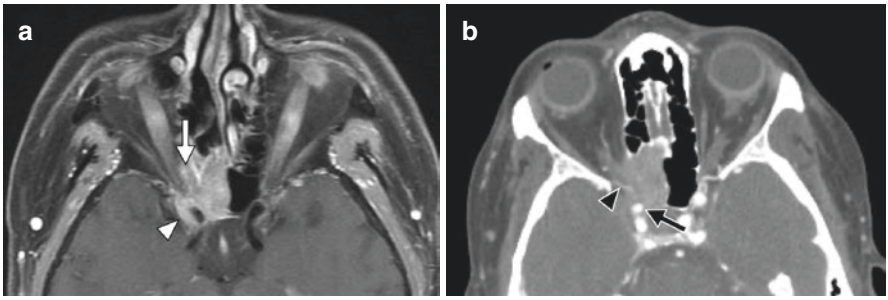

Fig. 2.6 Role of CT angiography. A 66-year-old woman with sinonasal undifferentiated carcinoma. (**a**) As seen on an axial T1-weighted fat-suppressed post-contrast MRI, the tumor invades from the right sphenoid sinus into the orbital apex (arrow) and right cavernous sinus (arrowhead). (**b**) For both preoperative planning and intraoperative guidance, CT angiography allows for clear delineation of the right internal carotid artery (arrow) and ophthalmic artery (arrowhead)

for intraoperative computer image guidance [25]. The relationship of the vascular anatomy with the tumor resection is then established, and this increases the extent of surgery that can be achieved with minimally invasive endoscopic endonasal approaches.

Magnetic Resonance Imaging

Magnetic resonance imaging (MRI) is an essential imaging modality in the assessment of almost all malignant and some benign sinonasal and skull base tumors. MRI offers superior soft tissue characterization and better defines the tumor extent when compared to CT. Differentiation of tumor from sinus obstruction/inflammation or mucocele is also better achieved with MRI. The range of imaging sequences offers superior soft tissue characterization with MRI, and allows identification of some specific histologies, although pathology is necessary for definitive diagnosis with the exception of angiofibroma. MRI is best used in combination with CT in order to achieve the highest yield for tumor identification and extent, surgical planning, and feasibility of resection.

Both pre- and post-contrast images with gadolinium-based intravenous contrast are generally obtained. Furthermore, interpretation of T1- and T2-weighted sequences can aid in differentiating tumor types, as well as delineating tumor from retained secretions in the paranasal sinuses. In the absence of hemorrhage or high protein content, retained secretions are hypointense on T1-weighted sequences and hyperintense on T2-weighted sequences, in contrast to tumor that is typically more T2 hypointense [10]. When trapped secretions become more proteinaceous and/or contain blood products, the T1 and T2 signals increase and decrease respectively (Fig. 2.7a–c). In addition to tumor type, tumor extension through orbital periosteum

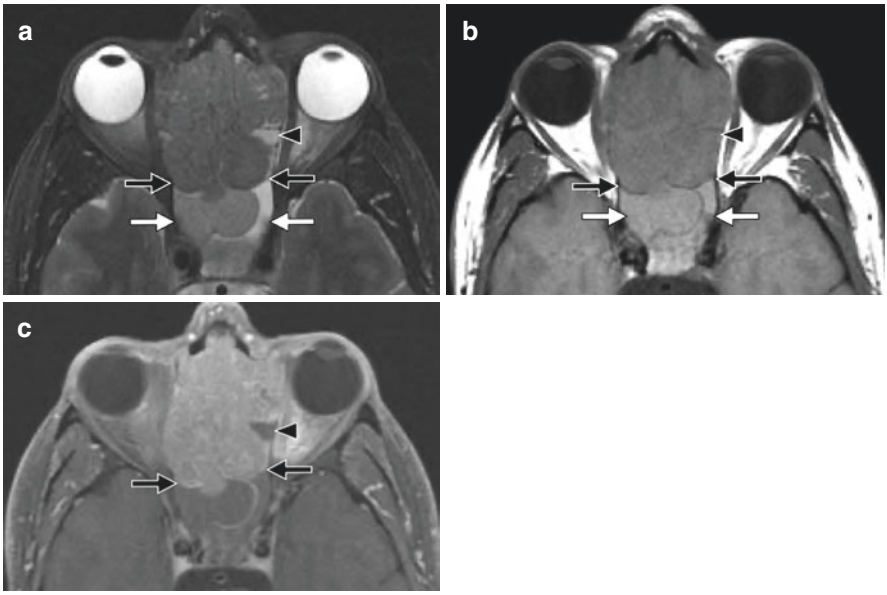

Fig. 2.7 Differentiating tumor from secretions with MRI. A 44-year-old woman with sinonasal diffuse large B-cell lymphoma. MRI sequences include: (**a**) axial fat-suppressed T2-weighted, (**b**) axial T1-weighted, and (**c**) axial fat-suppressed T1-weighted post-contrast. Note how signal characteristics of trapped secretions in the sphenoid sinuses (white arrows) and left ethmoid (black arrowhead) vary based on fluid content. Because of increased protein and/or blood products, both sphenoid sinuses are brighter than simple fluid on T1, while the ethmoidal secretions have intermediate T1 signal that blends with adjacent tumor. In contrast, the right sphenoid sinus is darker than the left on T2-weighted imaging. Although the posterior tumor margin (black arrows) is well defined on all three sequences, this is not always the case and can vary based on the signal characteristics of the retained secretions. At times, proteinaceous or hemorrhagic fluid can become extremely T1 hyperintense and therefore, blend imperceptibly with enhancing tumor. As a result, all MRI sequences must be reviewed in conjunction rather than solely relying on the T1-weighted post-contrast sequence

and dura is the most important prognostic factor (Fig. 2.8) [26]. Post-contrast T1-weighted images with fat suppression can identify tumor enhancement and invasion into the critical fat-containing regions of the orbit and pterygopalatine fossa. Intracranial extension may also be detected on post-contrast T1-weighted images with serial loss of the low signal intensity of the bone and cerebrospinal fluid (CSF) dividing the nasal cavity and paranasal sinuses from the intracranial contents. However, even the most detailed CT and MRI cannot always determine microscopic spread through periosteum and dura and frozen section may be required during surgery [3].

Abnormal enhancement of cranial nerves and loss of CSF within Meckel's cave on T2-weighted images may suggest perineural spread. Discontinuous enhancement along the nerve can be representative of skip lesions. Diffusion weighted imaging (DWI) and apparent diffusion coefficient (ADC) may be useful in

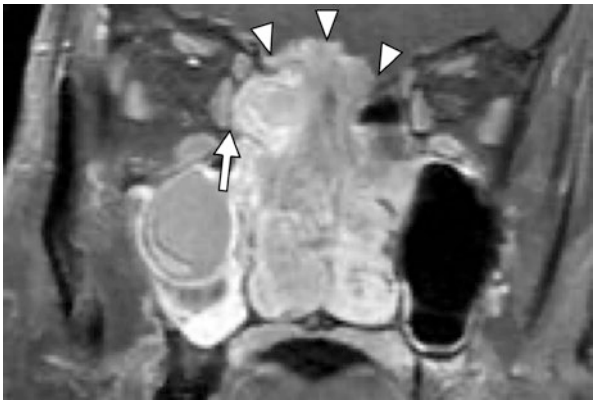

Fig. 2.8 Using MRI to assess intracranial and orbital invasion. A 41-year-old man with esthesioneuroblastoma. Coronal T1-weighted contrast-enhanced fat-suppressed MRI illustrates that a large sinonasal mass has invaded through the lamina papyracea into the medial right orbit, but a thin fat plane (arrow) still separates the tumor from the medial rectus muscle. The tumor has also invaded through the anterior skull base, and MRI can define the extent of dural involvement (arrowheads)

differentiating benign from malignant tumors, and also between malignant histologies [17, 27, 28]. The ADCs for benign sinonasal tumors have been found to be higher than in malignant lesions, with sensitivity and specificity over 80% [27, 28].

Characteristic MRI findings are found in several benign histopathologies. Inverted papilloma has a cerebriform or lobulated appearance on both T2-weighted and post-contrast T1-weighted images (Fig. 2.9a) [29]. Loss of cerebriform pattern within the tumor is suggestive of necrosis and should alert the clinician to the possibility of malignancy (Fig. 2.9b).

Fibro-osseous lesions can have a variable appearance on MRI, and overall are better visualized with CT. However, it should be recognized that fibrous dysplasia contains vascular tissue and therefore enhances on MRI (Fig. 2.9c), so an expansile osseous lesion on MRI should prompt further evaluation with CT, if not previously performed. Osteomas often appear homogeneous and hypointense on all MRI sequences when containing mostly dense cortical bone. Ossifying fibroma may appear hyperintense on T2-weighted sequences, particularly when predominantly composed of fibrous tissue. Juvenile angiofibroma will appear hypointense on T1-weighted images, but hyperintense on T2-weighted images. On post-contrast images, juvenile angiofibroma will have intense enhancement admixed with low-signal areas representative of flow-voids (Fig. 2.9d) [15]. Pleomorphic adenoma is typically associated with high signal intensity on T2-weighted images; however, sinonasal tumors typically arise from minor salivary gland and may have higher cellularity resulting in intermediate signal intensity [6, 10]. Distinctive characteristics of schwannoma include a “target” or “whorled” appearance on post-contrast images [10, 19].

Squamous cell carcinomas do not have specific MRI characteristics, although general signs for malignancy can be useful for determining tumor extent and stage.

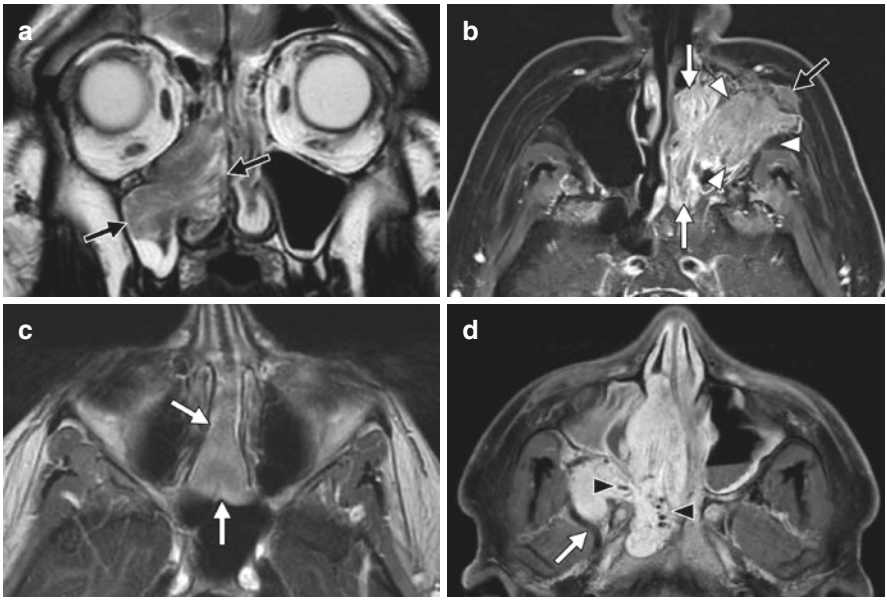

Fig. 2.9 MRI features of benign sinonasal masses/expansile lesions. (**a**) A 68-year-old man with inverted papilloma. Coronal T2-weighted MRI shows alternating hyperintense/hypointense curvilinear bands (arrows), which has been described as a convoluted cerebriform pattern. (**b**) A 61-year-old man with squamous cell carcinoma arising within an inverted papilloma. On post-contrast fat-suppressed T1-weighted MRI, the medial aspect of the mass in the nasal cavity has a convoluted cerebriform pattern suggesting inverted papilloma (white arrows). However, the lateral component of the mass (white arrowheads) is less avidly enhancing and lacks a striated appearance. Moreover, this component of the mass, which was found to represent squamous cell carcinoma, is behaving more aggressively with invasion through the anterior wall of the left maxillary sinus (black arrow). (**c**) A 21-year-old woman with sinonasal fibrous dysplasia. An expansile osseous lesion along the nasal septum and basisphenoid (arrows) is enhancing on this T1-weighted post-contrast MRI. Because fibrous dysplasia is often found incidentally on head MRI being performed for other reasons, this appearance should prompt correlation with CT because a characteristic ground-glass appearance on CT (see Fig. 2.4b) may obviate the need for biopsy. (**d**) A 16-year-old man with juvenile angiofibroma. Axial T1-weighted post-contrast MRI with fat suppression shows avid tumor enhancement and a very characteristic morphology/distribution with expansion of the sphenopalatine foramen/pterygopalatine fossa and extension into the infratemporal fossa. The flow-voids from the enlarged right internal maxillary artery (arrow) and dilated intratumoral vessels (arrowheads) are seen as dark curvilinear or dot-like structures, depending on their orientation relative to the plane of image acquisition

T2-weighted images often demonstrate intermediate signal intensity. Squamous cell carcinoma has also been shown to have higher ADCs than sinonasal lymphoma [17]. Invasion of the orbital or pterygopalatine fossa fat are important to identify, and can be assessed with post-contrast T1-weighted images with fat suppression. Intracranial extension is typically best viewed with post-contrast T1-weighted images as well. Adenocarcinoma remains essentially indistinguishable from squamous cell carcinoma by MRI features alone. Perineural invasion is an important

Fig. 2.10 MRI for the detection of perineural spread of sinonasal tumor. A 46-year-old man with left maxillary sinus squamous cell carcinoma. The coronal T1 post-contrast fat-suppressed MRI sequence nicely depicts extensive perineural spread involving the left trigeminal nerve. Tumor can be seen within the (**a**) infraorbital nerve (black arrowhead), (**b**) V2 division extending through foramen rotundum (black arrow), (**c**) Meckel's cave (white arrowhead), and (**d**) cisternal segment of the left trigeminal nerve (white arrow)

characteristic of adenoid cystic carcinoma, and may be seen in up to 50% of cases [30]. Evaluation of the full course of the cranial nerves is recommended due to the potential for skip lesions. Perineural spread is also commonly seen in squamous cell carcinoma, and should be considered in these tumors as well (Fig. 2.10a–d).

Olfactory neuroblastoma will have intermediate T1 signal and mild hyperintensity on T2-weighted images. Post-contrast enhancement can be variably homogeneous or heterogeneous. Cysts at the peripheral tumor margin are a characteristic finding of olfactory neuroblastoma (Fig. 2.11a), but these are only seen in a minority of cases [6]. This tumor may produce widespread separate dural deposits, so the entire cranial cavity must be imaged and carefully scrutinized (Fig. 2.11b) [31]. SNEC, SNUC, and NUT carcinoma are without specific MRI findings, although these tumors present with radiographic findings consistent with highly aggressive and invasive biologic behavior. Melanoma has been described to be hyperintense on T1-weighted images (Fig. 2.11c), although intermediate signal intensity is recognized as well.

Again, it is important to note that melanomas can appear disproportionately benign on imaging, including MRI.

Sinonasal lymphomas generally have low intensity on T2-weighted images (Fig. 2.11d) and appear as bulky masses. These tumors are more homogeneous than

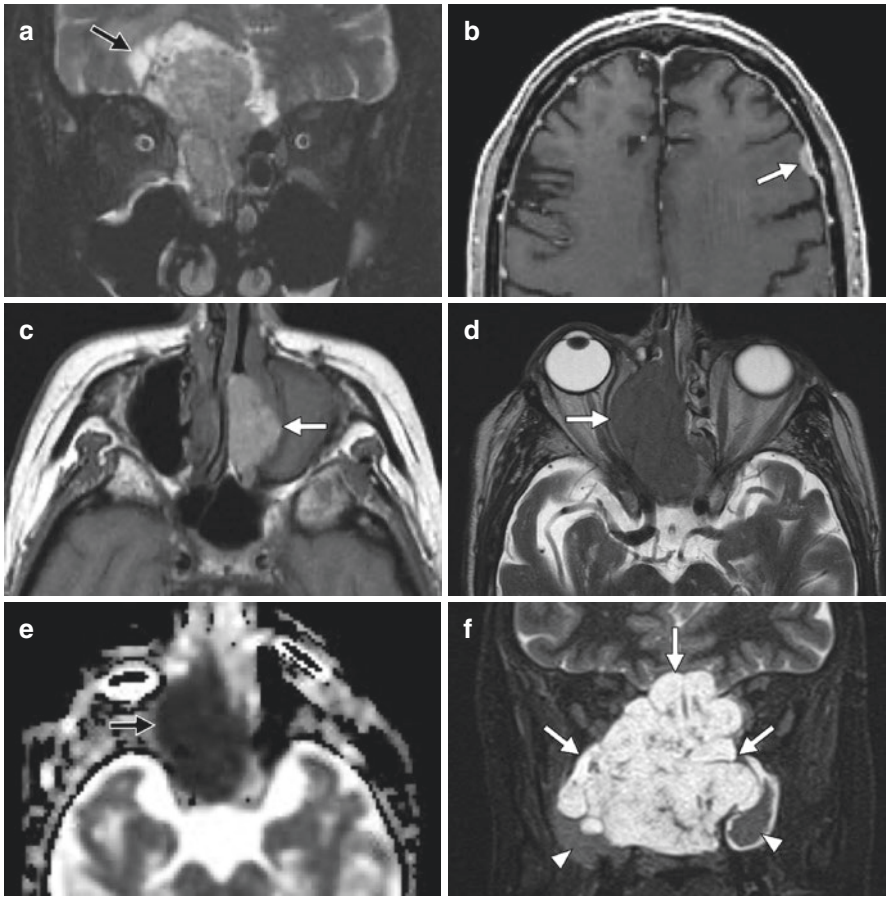

Fig. 2.11 MRI features of non-carcinomatous malignancies. (**a**) A 68-year-old man with esthesioneuroblastoma. As seen on a coronal T2-weighted MRI with fat suppression, a large superior right nasal mass has invaded intracranially with cyst formation at the interface between tumor and inferior frontal lobe (arrow). (**b**) A 72-year-old man with esthesioneuroblastoma. On surveillance imaging performed approximately 9 months following surgery, a small left frontal dural implant is identified on axial T1-weighted post-contrast MRI (arrow). (**c**) A 79-year-old woman with sinonasal melanoma. Axial T1-weighted MRI illustrates a left nasal mass smoothly remodeling the medial wall of the left maxillary sinus (arrow). The bright signal in the mass can be attributed to the intrinsic T1 hyperintensity of melanin, though prior intratumoral hemorrhage can also be contributory. (**d**) An 84-year-old man with diffuse large B-cell lymphoma. On axial T2-weighted MRI, a large right sinonasal mass is smoothly remodeling the lamina papyracea (arrow). Note that the mass has a very homogeneous appearance, which is more characteristic of lymphoma than carcinoma for a tumor of this size. In addition, the T2 signal of the mass is quite dark (similar to brain). Lymphoma is an example of a very cellular tumor with a high nuclear-to-cytoplasmic ratio, which leads to this pattern of T2 hypointensity in addition to a reduced apparent diffusion coefficient as seen in (**e**). (**f**) A 62-year-old woman with low-grade sinonasal chondrosarcoma. Coronal T2-weighted MRI with fat suppression shows the tumor to be markedly T2 hyperintense (arrows), similar to cerebrospinal fluid. Note how much brighter the tumor is compared with the proteinaceous secretions trapped in the maxillary sinuses (arrowheads)

squamous cell carcinoma on post-contrast T1- and T2-weighted images [17]. As noted previously the ADCs for sinonasal lymphoma are lower than squamous cell carcinoma, and are likely due to the higher cellularity of lymphomas (Fig. 2.11e) [17]. These characteristics can be helpful in differentiating sinonasal lymphomas from epithelial tumors and are relevant for surgical planning since chemotherapy is the primary treatment modality for lymphoma.

MRI features vary for sarcomas depending on the specific histopathology. Chondrosarcomas show high T2 signal (Fig. 2.11f) and low T1 intensity. These lesions enhance avidly on post-contrast images. Osteosarcoma also has low T1 signal intensity, although T2-weighted images are of intermediate intensity. Post-contrast images of osteosarcoma enhance less avidly than chondrosarcoma. MRI complements CT in evaluating the intramedullary and extraosseous extensions of osteosarcomas [6]. Rhabdomyosarcoma has intermediate signal intensity on all MRI sequences. Biphenotypic sinonasal sarcoma has shown mixed iso- and hypointensity on both T1- and T2-weighted images [23]. The majority of lesions demonstrated heterogeneous enhancement with gadolinium [23].

MRI has a role in post-treatment surveillance for sinonasal tumors (Figs. 2.1 and 2.2). The advantages of MRI in soft tissue characterization and multiple imaging sequences can also be applied to the post-treatment setting. The positive predictive value for tumor recurrence is reported to be as high as 84% [32], although there may be some interpretation-dependent variability [33]. The positive predictive value of MRI is higher than for CT, positron emission tomography (PET), and nasal endoscopy [32].

Positron Emission Tomography

The role of PET in the staging and surveillance of sinonasal malignancies is emerging. At present, morphological characterization of the local tumor is better achieved by traditional CT and MRI, although PET may be beneficial in the identification of synchronous lesions, as well as consolidating evaluation for regional and distant metastases into a single exam. PET imaging may also have a role in ongoing surveillance after treatment, in combination with physical exam and nasal endoscopy. PET imaging of the head and neck has been most commonly performed with ^{18}F-Fluoro-deoxy-glucose-PET (FDG-PET), and fused with CT images. Use of MRI with PET (PET/MRI) has also been investigated for use in sinonasal malignancies for superior soft tissue characterization of these tumors.

PET/CT

The utility of PET/CT in staging of sinonasal malignancies in comparison to standard CT and MRI is conflicting [34–36]. A recent study of 89 consecutive patients indicated a sensitivity of 81% and specificity of 99% for distant metastasis, and

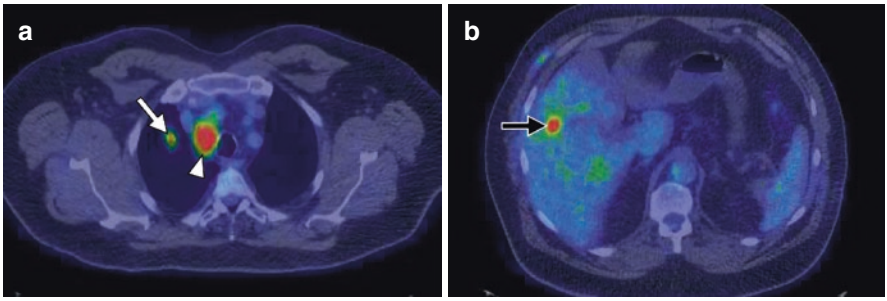

Fig. 2.12 Staging with PET/CT. A 61-year-old man with newly diagnosed sinonasal melanoma. Axial PET/CT images through the chest (**a**) and abdomen (**b**) demonstrate increased uptake of FDG in the right upper lobe (white arrow), superior mediastinum (arrowhead), and liver (black arrow) compatible with systemic metastases

sensitivity of 83% and specificity of 96% for regional nodal metastasis [34]. Second primary tumors were also detected in three patients [34]. Conversely, in an earlier study, PET/CT only resulted in upstaging in 1 of 47 patients [36]. Maximum standard uptake value (SUV) of the primary tumor was not correlated with the presence of metastatic disease [35]. A complicating factor of the studies examining the use of PET/CT for preoperative staging is the diversity of tumor histopathology. Given that the definitive diagnosis of the primary tumor will be made with pathology, PET/CT as a staging modality may be better reserved for aggressive pathologies with higher likelihood of metastasis (Fig. 2.12a, b). Alternative strategies for evaluation of distant and regional metastases include screening with CT of the neck and chest.

Use of PET/CT in the post-treatment surveillance of sinonasal malignancies has broader support in the literature, although specificity and positive predictive value remain poor [33, 37].

In a series of 34 patients with skull base malignancies, PET/CT was reported to have sensitivity and negative predictive value of 100%, while specificity was 40% and positive predictive value was 53.8% [37]. The poor specificity of PET/CT for disease recurrence is due to a relatively large number of false positives from post-treatment sinonasal inflammation. Conversely, negative PET/CT was highly predictive of a lack of recurrence, as evidenced by the high sensitivity and negative predictive value. Persistent sinonasal inflammation may require a different threshold SUV than other head and neck sites in order to improve specificity [33, 37]. In a separate study, the diagnostic yield of PET/CT for recurrence was highest at approximately 3 months and then after 18 months post-treatment [38].

PET/MRI

PET/MRI has been investigated for staging and determining resectability of head and neck cancers and sinonasal malignancies [39–41]. The suggested benefit of this modality is to combine the soft tissue detail of MRI with the ability of PET to

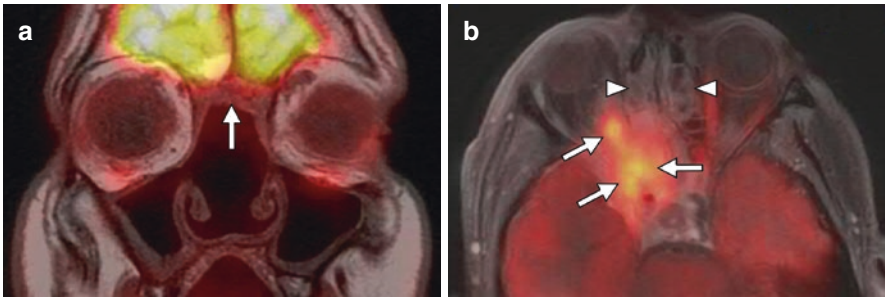

Fig. 2.13 Post-treatment assessment with PET/MRI. The simultaneous acquisition of PET and MRI allows for more accurate co-registration of the imaging data. (**a**) A 49-year-old man with history of treated esthesioneuroblastoma. PET co-registered with coronal T1-weighted MRI shows no evidence of increased FDG uptake in the operative bed (arrow) to suggest local tumor recurrence. (**b**) A 47-year-old man with a history of treated follicular dendritic cell sarcoma. PET co-registered with axial T1-weighted post-contrast fat-suppressed MRI demonstrates increased FDG uptake involving the right orbital apex, sphenoid sinus, and cavernous sinus in relation to recurrent tumor (arrows). Note that enhancing ethmoidal mucosa shows no evidence of abnormal radiotracer uptake (arrowheads) to raise suspicion

diagnose local and distant metastases. PET/MRI was reported to have similar sensitivity and specificity as PET/CT for identifying perineural and skull base invasion [39]. Diagnostic accuracy was also similar between both modalities in staging of head and neck cancers [40]. Data on the use of PET/MRI in the diagnosis, staging, and surveillance of sinonasal malignancies remain limited at this point and are not part of the standard evaluation of these tumors. Nevertheless, the combined advantages of PET and MRI imaging may be relevant for skull base tumors with increased experience with this modality (Fig. 2.13a, b).

Interventional Neuroradiology

Interventional neuroradiology is a consideration for certain tumor histologies or when there is involvement of the vascular anatomy. Angiography is useful for mapping vascular supply for juvenile angiofibroma (Fig. 2.14a) in addition to preoperative embolization of these tumors (Fig. 2.14b) [42, 43]. Complex involvement of the sinonasal and skull base vascular anatomies, which is incompletely assessed by other imaging modalities, may be an indication for angiography [24]. Balloon occlusion test, and possibly preoperative embolization, is also a consideration when there is substantial arterial encasement [24]. Finally, pseudoaneurysm formation is a potential post-treatment complication of sinonasal and skull base malignancies. Initial diagnosis can be made on CTA, although complete characterization requires angiography.

Endovascular interventions such as embolization or flow diversion are options for the treatment of pseudoaneurysms and can be performed in combination with angiography.

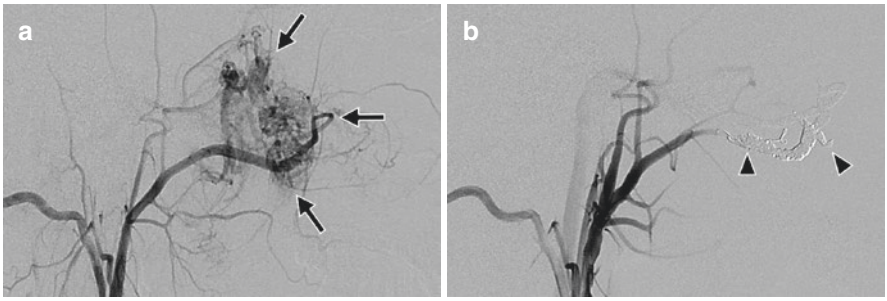

Fig. 2.14 Angiography and tumor embolization. A 16-year-old man with juvenile angiofibroma. (**a**) Lateral digital subtraction angiogram of the head (anterior corresponds to the right side of the image) via selective contrast injection into the right external carotid artery illustrates the extensive vascularity of the tumor (arrows), primarily derived from the internal maxillary artery. (**b**) Lateral digital subtraction angiogram of the head (anterior corresponds to the right side of the image) via selective contrast injection into the right external carotid artery demonstrates interval coil embolization (arrowheads) with tumor vascularity no longer apparent

Image-Guided Surgery

Intraoperative computer image guidance is an important consideration for the endoscopic endonasal resection of sinonasal malignancies. High-resolution CT images with axial slice thickness of 1 mm or less are used for computerized image guidance. CTA image sets can also be used for intraoperative surgical navigation for identification of important vascular structures [25]. Combined CT-MRI image guidance is also possible, where high-resolution MRI is automatically fused with CT images as the registration reference standard [44]. Fused CT-MRI navigation allows for the soft tissue detail of MRI to be used during resection of the tumor. Both intraoperative CT and MRI have been studied for possible improvements in the complete resection of skull base tumors by endoscopic approaches [45, 46]. While in a percentage of cases, information obtained from updated intraoperative images resulted in a decision for additional surgical resection, the routine use of these techniques is not currently supported.

References

1. El-Naggar AK, Chan JKC, Grandis JR, Takata T, Slootweg PJ. WHO classification of head and neck tumours. 4th ed. Lyon: International Agency for Research on Cancer; 2017. 347 p.
2. Bossi P, Farina D, Gatta G, Lombardi D, Nicolai P, Orlandi E. Paranasal sinus cancer. Crit Rev Oncol Hematol. 2016;98:45–61.
3. Lund VJ, Stammberger H, Nicolai P, Castelnuovo P, Beal T, Beham A, et al. European position paper on endoscopic management of tumours of the nose, paranasal sinuses and skull base. Rhinol Suppl. 2010;22:1–143.
4. Wang EW, Zanation AM, Gardner PA, Schwartz TH, Eloy JA, Adappa ND, et al. ICAR: endoscopic skull-base surgery. Int Forum Allergy Rhinol. 2019;9(S3):S145–365.

5. Rimmer J, Hellings P, Lund VJ, Alobid I, Beale T, Dassi C, et al. European position paper on diagnostic tools in rhinology. Rhinology. 2019;57(Suppl S28):1–41.
6. Madani G, Beale TJ, Lund VJ. Imaging of sinonasal tumors. Semin Ultrasound CT MR. 2009;30(1):25–38.
7. Lopez-Hernandez A, Perez-Escuredo J, Vivanco B, Garcia-Inclan C, Potes-Ares S, Cabal VN, et al. Genomic profiling of intestinal-type sinonasal adenocarcinoma reveals subgroups of patients with distinct clinical outcomes. Head Neck. 2018;40(2):259–73.
8. Capper D, Engel NW, Stichel D, Lechner M, Gloss S, Schmid S, et al. DNA methylation-based reclassification of olfactory neuroblastoma. Acta Neuropathol. 2018;136(2):255–71.
9. Dogan S, Vasudevaraja V, Xu B, Serrano J, Ptashkin RN, Jung HJ, et al. DNA methylation-based classification of sinonasal undifferentiated carcinoma. Mod Pathol. 2019;32(10):1447–59.
10. Agarwal M, Policeni B. Sinonasal neoplasms. Semin Roentgenol. 2019;54(3):244–57.
11. Eckhoff A, Cox D, Luk L, Maidman S, Wise SK, DelGaudio JM. Unilateral versus bilateral sinonasal disease: considerations in differential diagnosis and workup. Laryngoscope. 2020;130(4):E116–21.
12. Lee DK, Chung SK, Dhong HJ, Kim HY, Kim HJ, Bok KH. Focal hyperostosis on CT of sinonasal inverted papilloma as a predictor of tumor origin. AJNR Am J Neuroradiol. 2007;28(4):618–21.
13. Savy L, Lloyd G, Lund VJ, Howard D. Optimum imaging for inverted papilloma. J Laryngol Otol. 2000;114(11):891–3.
14. Agarwal M, Michel MA. Sino-orbital pathologies: an approach to diagnosis and identifying complications. Appl Radiol. 2017;46(8):8–20.
15. Lloyd G, Howard D, Lund VJ, Savy L. Imaging for juvenile angiofibroma. J Laryngol Otol. 2000;114(9):727–30.
16. Howard DJ, Lloyd G, Lund V. Recurrence and its avoidance in juvenile angiofibroma. Laryngoscope. 2001;111(9):1509–11.
17. Kim SH, Mun SJ, Kim HJ, Kim SL, Kim SD, Cho KS. Differential diagnosis of sinonasal lymphoma and squamous cell carcinoma on CT, MRI, and PET/CT. Otolaryngol Head Neck Surg. 2018;159(3):494–500.
18. Harbo G, Grau C, Bundgaard T, Overgaard M, Elbrond O, Sogaard H, et al. Cancer of the nasal cavity and paranasal sinuses. A clinico-pathological study of 277 patients. Acta Oncol. 1997;36(1):45–50.
19. McCollister KB, Hopper BD, Michel MA. Sinonasal neoplasms: update on classification, imaging features, and management. Appl Radiol. 2015;44(12):7–15.
20. Wormald R, Lennon P, O'Dwyer TP. Ectopic olfactory neuroblastoma: report of four cases and a review of the literature. Eur Arch Otorhinolaryngol. 2011;268(4):555–60.
21. Zanation AM, Ferlito A, Rinaldo A, Gore MR, Lund VJ, McKinney KA, et al. When, how and why to treat the neck in patients with esthesioneuroblastoma: a review. Eur Arch Otorhinolaryngol. 2010;267(11):1667–71.
22. Awad M, Gogos AJ, Kaye AH. Skull base chondrosarcoma. J Clin Neurosci. 2016;24:1–5.
23. Miglani A, Lal D, Weindling SM, Wood CP, Hoxworth JM. Imaging characteristics and clinical outcomes of biphenotypic sinonasal sarcoma. Laryngoscope Investig Otolaryngol. 2019;4(5):484–8.
24. Liu JK, Wong A, Eloy JA. Combined endoscopic and open approaches in the management of sinonasal and ventral skull base malignancies. Otolaryngol Clin N Am. 2017;50(2):331–46.
25. Leong JL, Batra PS, Citardi MJ. Three-dimensional computed tomography angiography of the internal carotid artery for preoperative evaluation of sinonasal lesions and intraoperative surgical navigation. Laryngoscope. 2005;115(9):1618–23.
26. Howard DJ, Lund VJ, Wei WI. Craniofacial resection for tumors of the nasal cavity and paranasal sinuses: a 25-year experience. Head Neck. 2006;28(10):867–73.
27. El-Gerby KM, El-Anwar MW. Differentiating benign from malignant sinonasal lesions: feasibility of diffusion weighted MRI. Int Arch Otorhinolaryngol. 2017;21(4):358–65.

28. Wang F, Sha Y, Zhao M, Wan H, Zhang F, Cheng Y, et al. High-resolution diffusion-weighted imaging improves the diagnostic accuracy of dynamic contrast-enhanced sinonasal magnetic resonance imaging. J Comput Assist Tomogr. 2017;41(2):199–205.
29. Hennessey PT, Reh DD. Benign sinonasal neoplasms. Am J Rhinol Allergy. 2013;27(3_suppl):S31–S4.
30. Bakst RL, Glastonbury CM, Parvathaneni U, Katabi N, Hu KS, Yom SS. Perineural invasion and perineural tumor spread in head and neck cancer. Int J Radiat Oncol Biol Phys. 2019;103(5):1109–24.
31. Rimmer J, Lund VJ, Beale T, Wei WI, Howard D. Olfactory neuroblastoma: a 35-year experience and suggested follow-up protocol. Laryngoscope. 2014;124(7):1542–9.
32. Khalili S, Worrall DM, Brooks S, Morris SM, Farquhar D, Newman JG, et al. Endoscopy versus imaging: analysis of surveillance methods in sinonasal malignancy. Head Neck. 2016;38(8):1229–33.
33. Workman AD, Palmer JN, Adappa ND. Posttreatment surveillance for sinonasal malignancy. Curr Opin Otolaryngol Head Neck Surg. 2017;25(1):86–92.
34. Ozturk K, Gencturk M, Rischall M, Caicedo-Granados E, Li F, Cayci Z. Role of whole-body (18)F-FDG PET/CT in screening for metastases in newly diagnosed sinonasal malignancies. AJR Am J Roentgenol. 2019;212(6):1–8.
35. Ramakrishnan VR, Lee JY, O'Malley BW Jr, Palmer JN, Chiu AG. 18-FDG-PET in the initial staging of sinonasal malignancy. Laryngoscope. 2013;123(12):2962–6.
36. Gil Z, Even-Sapir E, Margalit N, Fliss DM. Integrated PET/CT system for staging and surveillance of skull base tumors. Head Neck. 2007;29(6):537–45.
37. Harvey RJ, Pitzer G, Nissman DB, Buchmann L, Rumboldt Z, Day T, et al. PET/CT in the assessment of previously treated skull base malignancies. Head Neck. 2010;32(1):76–84.
38. Ozturk K, Gencturk M, Caicedo-Granados E, Li F, Cayci Z. Appropriate timing of surveillance intervals with whole-body (18)F-FDG PET/CT following treatment for sinonasal malignancies. Eur J Radiol. 2019;118:75–80.
39. Sekine T, Barbosa FG, Delso G, Burger IA, Stolzmann P, Ter Voert EE, et al. Local resectability assessment of head and neck cancer: positron emission tomography/MRI versus positron emission tomography/CT. Head Neck. 2017;39(8):1550–8.
40. Sekine T, de Galiza Barbosa F, Kuhn FP, Burger IA, Stolzmann P, Huber GF, et al. PET+MR versus PET/CT in the initial staging of head and neck cancer, using a trimodality PET/CT+MR system. Clin Imaging. 2017;42:232–9.
41. Meerwein CM, Hüllner M, Braun R, Soyka MB, Morand GB, Holzmann D. Current concepts in advanced sinonasal mucosal melanoma: a single institution experience. Eur Arch Otorhinolaryngol. 2019;276(8):2259–65.
42. Lopez F, Triantafyllou A, Snyderman CH, Hunt JL, Suarez C, Lund VJ, et al. Nasal juvenile angiofibroma: current perspectives with emphasis on management. Head Neck. 2017;39(5):1033–45.
43. Wu AW, Mowry SE, Vinuela F, Abemayor E, Wang MB. Bilateral vascular supply in juvenile nasopharyngeal angiofibromas. Laryngoscope. 2011;121(3):639–43.
44. Chiu AG, Palmer JN, Cohen N. Use of image-guided computed tomography-magnetic resonance fusion for complex endoscopic sinus and skull base surgery. Laryngoscope. 2005;115(4):753–5.
45. Batra PS, Manes RP, Ryan MW, Marple BF. Prospective evaluation of intraoperative computed tomography imaging for endoscopic sinonasal and skull-base surgery. Int Forum Allergy Rhinol. 2011;1(6):481–7.
46. Riley CA, Soneru CP, Tabaee A, Kacker A, Anand VK, Schwartz TH. Technological and ideological innovations in endoscopic skull base surgery. World Neurosurg. 2019:S1878-8750(19)30220-7. https://doi.org/10.1016/j.wneu.2019.01.120.